

Feedback Connections in Quantum Reservoir Computing with Mid-Circuit Measurements

Jakob Murauer*, Rajiv Krishnakumar†, Sabine Tornow* and Michaela Geierhos*

*Research Institute CODE, University of the Bundeswehr Munich, 85579 Neubiberg, Germany

†QuantumBasel, 4144 Arlesheim, Switzerland

Abstract—Existing approaches to quantum reservoir computing can be broadly categorized into restart-based and continuous protocols. Restart-based methods require reinitializing the quantum circuit for each time step, while continuous protocols use mid-circuit measurements to enable uninterrupted information processing. A gap exists between these two paradigms: While restart-based methods naturally have high execution times due to the need for circuit reinitialization, they can employ novel feedback connections to enhance performance. In contrast, continuous methods have significantly faster execution times but typically lack such feedback mechanisms. In this work, we investigate a novel quantum reservoir computing scheme that integrates feedback connections, which can operate within the coherence time of a qubit. We demonstrate our architecture using a minimal example and evaluate memory capacity and predictive capabilities. We show that the correlation coefficient for the short-term memory task on past inputs is nonzero, indicating that feedback connections can effectively operate during continuous processing to allow the model to remember past inputs.

Index Terms—quantum computing, quantum reservoir computing, mid-circuit measurements, dynamic circuits.

I. INTRODUCTION

Quantum computers have proven to provide significant speedups for specialized problems by exploiting the unique principles of quantum mechanics. These improvements are also thought to be valuable for machine learning tasks [1]–[4], although concrete evidence for an advantage is still a highly debated topic [5]. Quantum Reservoir Computing (QRC) is a promising approach in quantum machine learning with current noisy intermediate scale quantum hardware, due to an architecture that does not require expensive circuit optimization.

In particular, reservoir computing is a machine learning approach for predicting time series data [6]–[9]. A reservoir computer transforms an input sequence into a higher dimensional feature space by the use of a fixed but random non-linear system called a reservoir. A simple linear regression model is then trained to read the state of the reservoir and map the result to a desired output. Since the training is done only in the last stage, while the internal dynamics are fixed, the optimization is very efficient. QRC is the quantum analog of classical reservoir computing, where a quantum system is used as a reservoir and its complex dynamics are used to efficiently process temporal data [10]–[16]. This is seen as a promising approach because quantum systems offer a naturally high-dimensional Hilbert space and complex non-linear dynamics. These properties are thought to enhance the performance of reservoir computing [14], [17], [18].

Several architectures have been proposed, broadly categorized into restart-based and continuous methods. Conventional restart-based QRC schemes generate the output time series by averaging the measurement results across all qubits at each time step. This requires repeatedly re-preparing and running the system from the beginning for each time step to obtain the complete time series, see Fig. 1 (a). To avoid rerunning the entire process from the beginning, methods known as rewind protocols have been proposed [15]. Here, the reservoir for cycle k is initiated from cycle $k + 1 - \tau$ therefore reducing computation to the last τ cycles, as compared to the first cycle in the conventional approach (Fig. 1 (b)). This method is motivated by the fact reservoirs have a fading-memory property [19], which means that over time the reservoir loses information from distant timesteps, therefore making them insignificant for newer cycles. On the other hand, continuous QRC methods leverage mid-circuit measurements to continuously monitor the dynamics of the reservoir, Fig. 1 (d), improving overall execution time on quantum hardware immensely [20]. This method has also been combined with weak measurements to mitigate the erasure of past inputs, as they extract limited information without fully collapsing the quantum state. However, this comes at a cost, as the readout from the reservoir is now incomplete [15].

A novel approach introduces a feedback link by feeding back expectation values into the reservoir [14]. This approach still restarts for each time step, but only needs to run for one time step at a time. While this method effectively incorporates memories of previous inputs into the reservoir, it still has a drawback, namely execution time on quantum hardware. As shown in Fig. 1 (d), for each time step the expectation value must be estimated with a certain number of shots.

In this paper we introduce a novel feedback driven quantum reservoir computing approach with mid circuit measurements and classical feedforward operations during the coherence time of a qubit. As seen in Fig. 1 (d), each cycle requires n shots. Thus, for an input sequence with a training length t tested over k different values, the total number of shots scales with $t \times k \times n$. As t , k , or preferably n grow, the cumulative cost of running these circuits becomes large. This motivates our exploration of feedback connections that operate within a qubit’s coherence time, using novel classical feedforward methods. To isolate and rigorously quantify the effect of the mid-circuit feedback, we perform a qubit reset after each time step. This ensures no extraneous information (other than

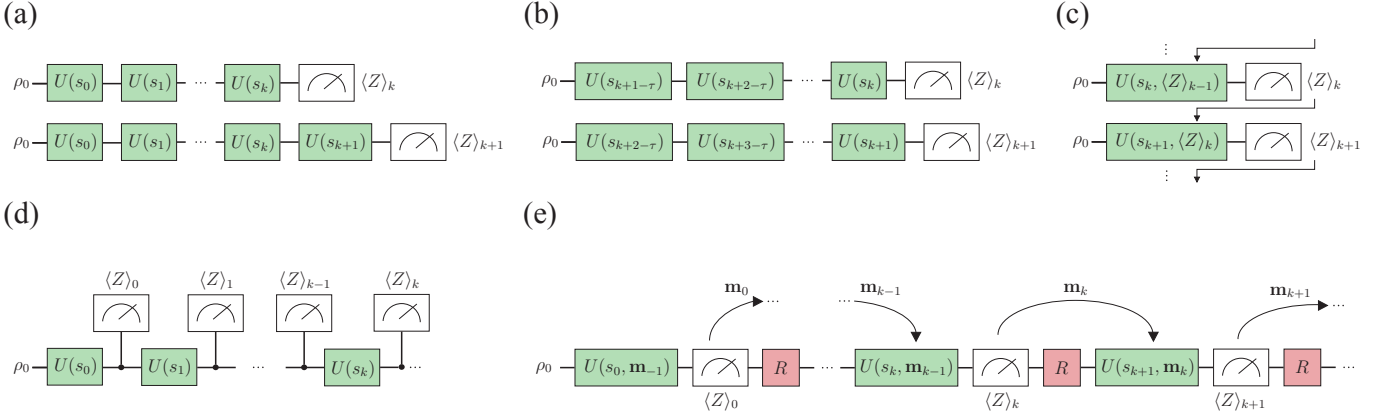


Fig. 1. **Quantum reservoir computing protocols:** Each architecture is designed to process an input sequence s_k . The systems are initialized in the state $\rho_0 = |0\rangle\langle 0|$. A unitary operator $U(\cdot)$ constructed from parametrized Pauli rotations, governs the state evolution. Each $U(\cdot)$ represents the processing of one timestep (cycle). **(a)** Graphical representation of a conventional restart based QRC regime. For each timestep the architecture needs to be restarted and run from the beginning. This amounts to a quadratic runtime. **b** A rewind protocol, that is not restarted from the beginning, but only processes the last τ timesteps. **c** A feedback driven QRC protocol. Only one timestep is processed at a time, but the expectation value from the previous experiment is put into reservoir. **d** A mid-circuit measurement architecture, that continuously monitors the quantum state. No restarting is needed. This architecture can be combined with weak measurements. **d** A feedback driven QRC architecture with mid-circuit measurements. Feedback is incorporated by feeding the measurement strings \mathbf{m}_k back into the reservoir, a process that can be performed at runtime.

the intended feedback) propagates forward, allowing us to examine the feedback connection itself in a controlled manner. One may omit these resets to explore more complex scenarios in which correlations persist over time, but here our primary goal is to study feedback connections in isolation, thereby clarifying their impact. For implementation, IBM superconducting systems have notably demonstrated real-time classical feedforward operations [21], offering an option to reduce the overall shot overhead for certain problems. We use the measurement strings obtained through a mid-circuit measurement as feedback for the next cycle. We can tune the feedback strength and the input strength through hyperparameters. We evaluate the memory performance through investigation of the short-term memory task and evaluate the predictive capabilities with the prediction of the Mackey-Glass system [22] and the expectation value of one spin in a chaotic Ising chain.

II. METHODS

A. Architecture

We propose a QRC architecture with mid-circuit measurements, that incorporates feedback connections, as depicted in Fig. 1 (e). We start with a N qubit quantum system, initialized in the state $\rho_0^N = |0\rangle\langle 0|^{\otimes N}$. Given an input sequence s_k , the system evolution is governed by the unitary operator $U(s_k, \mathbf{m}_{k-1})$, where s_k is the current timestep of the input sequence and $\mathbf{m}_{k-1} \in \{-1, 1\}^N$ is previous measurement results of cycle s_{k-1} . The input sequence is placed into a two qubit gate $R(a_{in}s_k)$, whereas each previous measurement result m_{k-1}^j is inserted into another two qubit gate $R(a_{fb}m_i^j)$. The structure of the R gate is defined as:

$$R_{i,j}(\theta) = CX_{ij}RZ_j(\theta)CX_{ij}RX_j(\theta)RX_i(\theta) \quad (1)$$

Here, θ represents an angle parameter that determines the rotation applied in the two-qubit gate. Specifically, θ can take

values from the set $\{a_{in}s_k, a_{fb}m_{k-1}^j\}$ where a_{fb} and a_{in} are scaling parameters in \mathcal{R} , that allow to control the input and feedback strength. We want to add that this structure is an usual reservoir structure found in QRC literature [14], [20], [23]. The full unitary $U(s_k, \mathbf{m}_{k-1})$ consists of one input R gate, N feedback R gates and one Haar random unitary. The idea is illustrated for the 2 qubit case in Fig. 2. For the first timestep s_0 a random vector \mathbf{m}_{-1} uniformly distributed from $\{-1, 1\}^N$ is selected for timestep 0. After unitary evolution the system is projectively measured in computational basis. We reset our system to ρ_0^N and feed the measurement string forward into the next unitary.

B. Training

The task of quantum reservoir computing is defined by an input sequence $\{s_k\}$ and a target sequence $\{\hat{y}_k\}$. The goal is to build a regression model that accurately approximates the target sequence. In typical quantum reservoir computing mechanisms, there are three main stages: washout, training, and testing. As discussed in Section II-A, we begin the first cycle s_0 with a randomly selected feedback vector. To remove the effects of this initialization, we discard the first l_w measurement outcomes (the *washout* phase). Subsequently, the following l_{tr} steps are used to train the model (the *training* phase), and performance is then evaluated on the next l_{ts} steps (the *testing* phase). The linear regression model is then build based on the following reservoir outputs. Specifically we build the matrix $X_{tr} \in \mathcal{R}^{l_{tr} \times (N+1)}$ defined as:

$$X_{tr} = \begin{bmatrix} \langle Z \rangle_{lw+1}^1 & \langle Z \rangle_{lw+1}^2 & \cdots & \langle Z \rangle_{lw+1}^N & 1 \\ \langle Z \rangle_{lw+2}^1 & \langle Z \rangle_{lw+2}^2 & \cdots & \langle Z \rangle_{lw+2}^N & 1 \\ \vdots & & & & \\ \langle Z \rangle_{lw+ltr}^1 & \langle Z \rangle_{lw+ltr}^2 & \cdots & \langle Z \rangle_{lw+ltr}^N & 1 \end{bmatrix} \quad (2)$$



Fig. 2. Minimal two-qubit unitary circuit. The circuit processes the input s_k through a rotation $R(a_{in} s_k)$ and then incorporates feedback via rotations $R(a_{fb} m_{k-1}^0)$ and $R(a_{fb} m_{k-1}^1)$, where $\{m_{k-1}^0, m_{k-1}^1\}$ are the prior measurement outcomes. The structure of $R(\cdot)$ is explained in Eq. 1. A final Haar-random unitary U_{Haar} is applied at the end.

where $\langle Z \rangle_k^n$ is the expectation value of the Pauli Z operator on the n th qubit at the k th timestep.

We create now a linear model w_{opt} such that $y_{tr} = X_{tr} w_{opt}$ closely resembles the target sequence \hat{y}_{tr} . We utilize Moore-Penrose pseudoinverse:

$$w_{opt} = (X_{tr}^T X_{tr})^{-1} X_{tr}^T \hat{y}_{tr} \quad (3)$$

C. Testing

The testing routine largely follows the training routine; however, instead of creating a new model, we use the existing model to obtain a prediction vector of length l_{ts} . We create a matrix $X_{ts} \in \mathcal{R}^{l_{ts} \times (N+1)}$ defined as:

$$X_{ts} = \begin{bmatrix} \langle Z \rangle_{lw+ltr+1}^1 & \dots & \langle Z \rangle_{lw+ltr+1}^N & 1 \\ \langle Z \rangle_{lw+ltr+2}^1 & \dots & \langle Z \rangle_{lw+ltr+2}^N & 1 \\ \vdots & & & \\ \langle Z \rangle_{lw+ltr+lts}^1 & \dots & \langle Z \rangle_{lw+ltr+lts}^N & 1 \end{bmatrix} \quad (4)$$

The prediction vector in terms of w_{opt} is then given as:

$$y_{pred} = X_{ts} w_{opt} \quad (5)$$

The resulting prediction y_{pred} is then compared against the target vector \hat{y}_{ts} to assess the model's predictive performance.

III. EXPERIMENTS

A. Short-term memory capacity

To characterize the performance of remembering past inputs we use the short-term memory capacity [24]. Consider an input sequence $\{s_k\}$, where each s_k is drawn independently from a uniform distribution on $[0, 1]$. The objective is to retrieve past values of the sequence, formulated as $\hat{y}_k = s_{k+\tau}$, where τ is zero or negative. This metrics then utilizes the square of the correlation coefficient between the predicted target and real target:

$$R_\tau^2 = \frac{\text{cov}^2(\hat{y}_{ts}, y_{pred})}{\sigma^2(\hat{y}_{ts}) \sigma^2(y_{pred})} \quad (6)$$

When R_τ^2 is near 1, the model's predictions align closely with the actual target values, indicating minimal error. In contrast, when R_τ^2 is close to 0, the predicted outputs show substantial divergence from the true targets. The short-term memory capacity is then measured by summing up R_τ^2 for various steps:

$$C_\Sigma = \sum_\tau R_\tau^2 \quad (7)$$

B. Predictive Capabilities

To evaluate predictive capabilities we test the model on one classical task and one quantum time series. For the study of classical dynamical systems, we select the Mackey-Glass time series, a well-known benchmark that has been extensively in the context of reservoir computing [10], [14], [25], [26]. The delay differential equation is defined as [22]:

$$\frac{dP(t)}{dt} = \frac{\beta_0 \theta^n P(t - \tau)}{\theta^n + P(t - \tau)^n} - \gamma P(t) \quad (8)$$

We set $\beta_0 = 0.2$, $\theta = 1$, $n = 10$, $\tau = 17$ and $\gamma = 0.1$. To generate the time series, we numerically integrate the delay differential equation using a forward Euler scheme with a time step $\Delta t = 1$. The initial values are set to a constant for the duration of the delay, and the trajectory is normalized to the interval $[0, 1]$.

The quantum time series is constructed from the expectation value of the middle spin's σ^z operator in a one-dimensional Ising chain governed by the Hamiltonian

$$H = J \sum_i \sigma_i^z \sigma_{i+1}^z + h_x \sum_i \sigma_i^x + h_z \sum_i \sigma_i^z \quad (9)$$

We simulate the system using this Hamiltonian with parameters set to $N = 5$, $J = 1$, $h_x = 1.05$, and $h_z = -0.5$. At this parameter set the quantum Ising model becomes non integrable and exhibits chaotic behavior [27]. At each timestep, the expectation value $\langle Z_t^2 \rangle$ of the central spin is measured, generating the time series. The time evolution is discretized with a timestep of $\Delta t = 0.005$.

For all predictive tasks the goal is to forecast steps in the future, similarly formulated with the target sequence as $\hat{y}_k = s_{k+\tau}$, where τ is positive. We evaluate the models performance with the norm mean squared error, which is defined as:

$$\text{NMSE}(\hat{y}_{ts}, y_{pred}) = \frac{\sum_{i=1}^N (\hat{y}_{ts,i} - y_{pred,i})^2}{\sum_{i=1}^N (\hat{y}_{ts,i})^2} \quad (10)$$

The NMSE measures the size of the error relative to the scale (magnitude) of the true data. A low error indicates a good performance of the model, whereas high values indicate a large deviation from the target sequence.

C. Analysis of Echo State Property

As previously mentioned in section I, one of the important aspects of a reservoir computing model is the so called fading-memory property. In the classical setting of echo state network (ESN) reservoir computing models, this can be implemented by assuring that the ESN contains the echo state property (ESP) [28], which ensures that the internal state of the model becomes asymptotically dependent on only the input history regardless of its initial conditions. However in quantum reservoir computing models, the fading-memory property is usually generated by including some (preferably controlled) dissipation into the model [29], [30]. Therefore the importance of the ESP in quantum reservoir models is still unclear.

As a first step into investigating the role of the ESP in quantum reservoir computing models, we perform an analysis of the asymptotic dependency of the reservoir state of several reservoir computing models (including the one proposed in this paper) with respect to their initial internal states. To do this, we look at how the internal state of the reservoir evolves over time across different scenarios of random initializations of the reservoir state. We can define the internal state of the reservoir $x_t \in \mathcal{R}^M$ at time t to be:

$$x_t = F(x_{t-1, s_t}) \quad (11)$$

where M is the reservoir dimension, F is the fixed reservoir function and s_t is the time series at time t [19], [28].¹ For each model, we use input sequences drawn from a uniform distribution on $[0, 1]$ (as described in Section III-A) across 5 random initializations. For each run, we extract the first component of the reservoir's internal state, x_t^1 , at time t and track its evolution over time across the different runs. To quantify the asymptotic behavior of these internal states, we compute the average difference of the feature across runs. We perform this analysis for a classical minimal ESN model [31], a feedback-driven QRC protocol [14], a QRC scheme with a mid-circuit measurement architecture [20], and the model proposed in this paper.

IV. RESULTS AND DISCUSSION

We obtain all predictive and memory related results by simulating a minimal instance of the proposed architecture with a system size of $N = 2$. While we do use a density matrix formalism, accounting for all possible measurement trajectories under the conditional feedforward mechanism would require exponential overhead and is therefore not feasible. Instead, we employ a shot-based approach, in which each shot represents a single experiment on quantum hardware, and individual measurement outcomes are sampled directly. For further computational efficiency, we choose a washout length $l_w = 25$, training length $l_{\text{tr}} = 100$, and test length $l_{\text{ts}} = 100$.

In Fig. 3 (a) on the right, we present the short-term memory correlation coefficient for four different delay values. Even with a limited number of shots, the minimal example exhibits nonzero correlation coefficients for $\tau = 1$, indicating that the fundamental feedback connections during continuous processing play a beneficial role for memory. Notably, the feedback connections were evaluated using a reset operation after each measurement, ensuring that any information transmitted forward originates solely from the proposed mechanism. Furthermore, an upward shift is observed for an increasing number of shots, suggesting that performance improves with additional measurement statistics. On the left in 3 (a), we show the effect of varying the feedback strength on the memory capacity C_Σ for different numbers of measurements for a fixed $a_{fb} = 1.3$. We observe again an upward shift in performance with an increasing number of measurement shots. Notably we think that careful tuning of both the feedback and input strengths

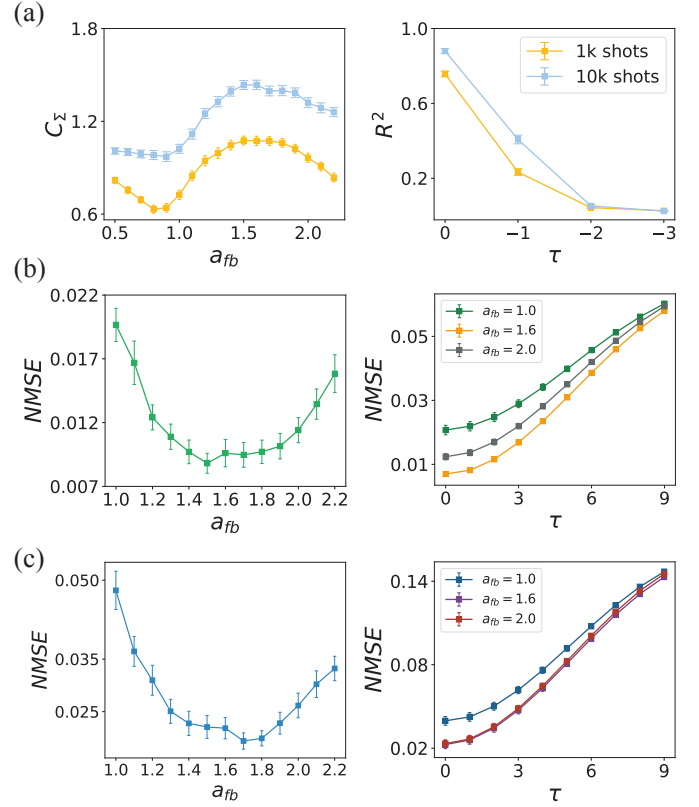


Fig. 3. **Evaluation of short term memory and predictive capabilities:** All values are averaged over 128 Haar-random unitaries. Since there is no single ‘privileged’ choice of unitary, our primary interest is the mean performance of the protocol over these random instances. We therefore report the standard error of the mean to reflect how much this mean would vary if we resampled from the Haar measure many times. (a) The left panel shows the short-term memory (STM) capacity for several different values of a_{fb} , with τ ranging from 0 to -3 . The right panel provides a more detailed view for $a_{fb} = 1.3$, plotting all values of τ . (b) Here we display the NMSE for the quantum 1D Ising chain, showing predictive capabilities for $\tau = 1$ across various a_{fb} values. The right panel presents predictive capabilities for different τ values for selected a_{fb} values. Figure (c) shows the same analysis for the Mackey-Glass task. For both (b) and (c), 5k shots were used.

is crucial for robust performance as well as the right choice of the Haar matrix. As noted in [14], when the angles in the feedback and input R gates exceed $\pm 2\pi$, the reservoir fails to process the feedback connections reliably, causing the memory capacity to vanish. From the evaluation in Fig. 3 (a) we can see, that there is an increase in memory capacity for a_{fb} values from 1.0 to around 2.0. Interestingly, this trend is also reflected in the predictive performance — lower NMSE values are observed for the same a_{fb} range, as illustrated in Fig. 3 (b) and (c). This again affirms the importance of memory capacity for predictive tasks. We can report an overall minimal average NMSE of 8.8×10^{-3} on the 5-qubit Ising chain. The model performs slightly worse on the classical dynamical MG sequence with a minimal average NMSE of 1.9×10^{-2} .

We now present the results from the experiment on the analysis of the echo state property of different reservoir computing models as described in subsection III-C. In all methods, we replicate the reservoirs as described in their

¹In our architecture $x_t = [\langle Z \rangle_t^1, \langle Z \rangle_t^2, \dots, \langle Z \rangle_t^N]$

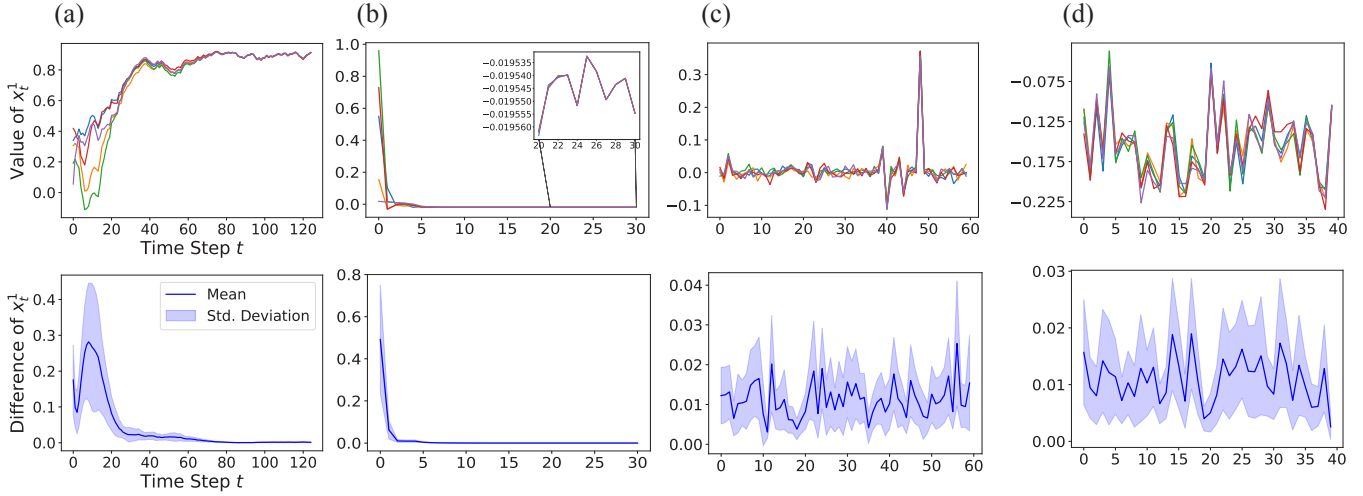


Fig. 4. **Echo state property for various architectures:** The top figures show the first element of the reservoir state over time for five randomly initialized runs, while the bottom figures present the absolute difference among these five reservoir states. (a) Classical ESN model. (b) Feedback driven QRC regime [14]. (c) Mid-circuit measurement QRC [20]. (d) Our algorithm.

respective references. In particular:

- For the classical minimal ESN model - we use a network of the form

$$x_{t+1} = (1 - \alpha)x_t + \alpha \tanh(W_{in}s_t + b + Wx_t) \quad (12)$$

where x_k contains 1000 dimensions, each element in W_{in} , b and W are initialized with the random variable $X \sim \mathcal{N}(-0.5, 1)$ in addition to which W is then renormalized to have a spectral radius of 1.25, and $\alpha = 0.3$. This configuration replicates a model that was able to accurately reproduce the Mackey-Glass trajectory with a delay value τ of 17 in an auto-regressive manner for over 2000 steps after the training cycle. Each run was performed with a different initialization of x_0 , with each parameter randomly chosen from a uniform distribution between 0 and 1.

- For the feedback driven QRC protocol - we take the architecture proposed in Fig. 1 (c) in Ref. [14] with the hyperparameters $a_{in} = 0.001$, $a_{fb} = 2.5$ and a Haar-randomly chosen U_{res} , and using a statevector simulator to compute the expectation values of the measurements. This configuration replicates the model used to produce the results in the reference. Each run was performed with a different initialization of the initial feedback vector, with each component randomly chosen from a uniform distribution between 0 and 1.
- For the QRC scheme with a mid-circuit measurement architecture - we take the architecture proposed in Fig. 1 (d) in Ref. [20] with 10 time-steps and setting $a = 5$ and 10^4 shots². This model requires no random initializations.

²although no specific value for a was explicitly stated in the original work, we were able to reproduce the NARMA2 benchmark results when setting $a = 5$

- For the model proposed in this paper - we use the model described in Fig. 1 (e) with $a_{in} = 1$, $a_{fb} = 1.6$, a Haar-randomly chosen U_{Haar} and 10^4 shots. This configuration maximized the short-term memory capacity as shown in Fig 3 (a). Each run was performed with a different initialization of the initial random feedback vector \mathbf{m}_{-1} .

The results of the ESP analysis can be found in Fig. 4. We notice that the classical minimal ESN model and the feedback driven QRC protocol model both clearly display the echo-state property, see Fig. 4 (a) and (b). On the other hand, we see that the QRC scheme with a mid-circuit measurement architecture and the model we propose do not display reservoirs that are asymptotically independent of the initial state. However, the QRC scheme with a mid-circuit measurement architecture, despite not having an echo state property, was shown to be successful at reproducing NARMA time-series benchmarks and to maybe even have a promise in modeling soft robots [20]. Therefore the relationship between the asymptotic behavior of a quantum reservoir state with respect to its initial conditions vs the reservoir model having the fading-memory property does not seem to be as straightforward for the QRC models as it is for their classical counterparts. To ensure we did not happen to fall upon a special case, we repeated the analysis with several different initializations of the fixed random parameters (e.g. W_{in} , U_{Haar} , etc.) and across different dimensions of the internal state of the reservoir, which led to qualitatively similar results as the ones shown in Fig. 4.

V. CONCLUSION

In this paper, we propose a quantum reservoir computing scheme that uses mid-circuit measurements and feedback within the runtime time of a qubit. Our initial experiments aim to determine whether feedback connections during runtime genuinely improve memory capacity rather than merely

introducing uncertainties due to measurement noise. We show that an architecture of this type with incorporated resets exhibits nonzero memory capacity for past inputs, indicating that feedback connections have an impact. Notably, peaks in memory capacity at specific feedback strengths align with enhanced performance on predictive tasks involving both classical and quantum chaotic systems. Our ESP findings reveal that while the classical minimal ESN model and the feedback-driven QRC protocol both exhibit clear echo-state behavior, mid-circuit measurements QRC schemes can remain effective despite lacking this property. Nonetheless, we strongly think that this idea is yet not fully explored. Further investigation could involve experimenting with alternative reset strategies, such as using conditional resets or omitting resets entirely, thus allowing the model to continue its evolution from the post-measurement state, while additionally having feedback connections. We have also not yet explored scaling the system size, which is an is promising direction for future investigation that can unveil scaling capacities of this approach. Finally, the most important next step is to implement this approach on actual quantum hardware. As noted in Section I, the IBM platform supports mid-circuit measurements with classical feedforward operations, but these are currently limited to 50 operations per circuit. This constraint will likely be eased in the future, particularly as error-correcting protocols become more prevalent. We would also like to suggest to dive deeper in the underlying importance of the Haar random unitary in QRC schemes.

APPENDIX A NOISE TEST

Here we present some preliminary noise tests. In our numerical shot based simulation we introduce a depolarization channel after each unitary of the form:

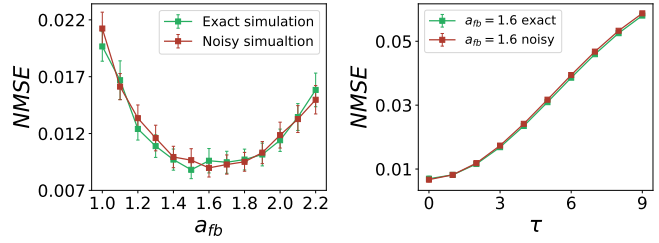
$$DP(\rho) = (1 - \lambda)\rho + \lambda \frac{I}{d} \quad (13)$$

where λ is the probability of the state to be found in the completely mixed state $\frac{I}{d}$. For the one qubit case, the DP channel can expressed also with the Kraus operators

$$K_0 = \sqrt{1 - \frac{3\lambda}{4}}I, K_1 = \sqrt{1 - \frac{\lambda}{4}}X, \quad (14)$$

$$K_2 = \sqrt{1 - \frac{\lambda}{4}}Y, K_3 = \sqrt{1 - \frac{\lambda}{4}}Z \quad (15)$$

We set lambda to 0.04, which corresponds geometrically to a uniformly Bloch sphere reduction of 4%, or in terms of random processes: With 97% chance, we apply the identity. With 1% chance each, we apply X , Y or Z . We now look at the predictive capabilities on the Ising chain, similar to Fig. 3 (b). This preliminary finding suggests that our architecture exhibits noise resistance. Investigation will go into the explanation of why this is the case.



APPENDIX B CODE AVAILABILITY

The Python implementation to reproduce the results can be found at <https://github.com/Muri7910/Feedback-Connections-in-Quantum-Reservoir-Computing-with-Mid-Circuit-Measurements>. Further information and data is available upon reasonable request.

REFERENCES

- [1] M. Schuld and F. Petruccione, *Machine learning with quantum computers*, 2nd ed., ser. Quantum Science and Technology. Cham, Switzerland: Springer Nature, Oct. 2021.
- [2] N. Wiebe, D. Braun, and S. Lloyd, “Quantum algorithm for data fitting,” *Phys. Rev. Lett.*, vol. 109, no. 5, p. 050505, Aug. 2012.
- [3] J. Biamonte, P. Wittek, N. Pancotti, P. Rebentrost, N. Wiebe, and S. Lloyd, “Quantum machine learning,” *Nature*, vol. 549, no. 7671, pp. 195–202, Sep. 2017.
- [4] M. Periyasamy, A. Plinge, C. Mutschler, D. D. Scherer, and W. Mauerer, “Guided-spса: Simultaneous perturbation stochastic approximation assisted by the parameter shift rule,” in *2024 IEEE International Conference on Quantum Computing and Engineering (QCE)*, vol. 01, 2024, pp. 1504–1515.
- [5] J. Bowles, S. Ahmed, and M. Schuld, “Better than classical? the subtle art of benchmarking quantum machine learning models,” 2024. [Online]. Available: <https://arxiv.org/abs/2403.07059>
- [6] C. Wringe, M. Trefzer, and S. Stepney, “Reservoir computing benchmarks: a tutorial review and critique,” *arXiv [cs.ET]*, 2024.
- [7] M. Dale, S. O’Keefe, A. Sebald, S. Stepney, and M. A. Trefzer, “Reservoir computing quality: connectivity and topology,” *Nat. Comput.*, vol. 20, no. 2, pp. 205–216, Jun. 2021.
- [8] X.-Y. Duan, X. Ying, S.-Y. Leng, J. Kurths, W. Lin, and H.-F. Ma, “Embedding theory of reservoir computing and reducing reservoir network using time delays,” *Phys. Rev. Res.*, vol. 5, p. L022041, May 2023. [Online]. Available: <https://link.aps.org/doi/10.1103/PhysRevResearch.5.L022041>
- [9] M. Dale, J. F. Miller, S. Stepney, and M. A. Trefzer, “A substrate-independent framework to characterize reservoir computers,” *Proc. Math. Phys. Eng. Sci.*, vol. 475, no. 2226, p. 20180723, Jun. 2019.
- [10] K. Fujii and K. Nakajima, “Harnessing disordered-ensemble quantum dynamics for machine learning,” *Phys. Rev. Appl.*, vol. 8, p. 024030, Aug 2017. [Online]. Available: <https://link.aps.org/doi/10.1103/PhysRevApplied.8.024030>
- [11] A. Senanian, S. Prabhu, V. Kremenski, S. Roy, Y. Cao, J. Kline, T. Onodera, L. G. Wright, X. Wu, V. Fatemi, and P. L. McMahon, “Microwave signal processing using an analog quantum reservoir computer,” *Nat. Commun.*, vol. 15, no. 1, p. 7490, Aug. 2024.
- [12] D. Fry, A. Deshmukh, S. Y.-C. Chen, V. Rastunkov, and V. Markov, “Optimizing quantum noise-induced reservoir computing for nonlinear and chaotic time series prediction,” *Sci. Rep.*, vol. 13, no. 1, p. 19326, Nov. 2023.
- [13] J. Dudas, B. Carles, E. Plouet, F. A. Mizrahi, J. Grollier, and D. Marković, “Quantum reservoir computing implementation on coherently coupled quantum oscillators,” *Npj Quantum Inf.*, vol. 9, no. 1, Jul. 2023.
- [14] K. Kobayashi, K. Fujii, and N. Yamamoto, “Feedback-driven quantum reservoir computing for time-series analysis,” *PRX quantum*, vol. 5, no. 4, Nov. 2024.

- [15] P. Mujal, R. Martínez-Peña, G. L. Giorgi, M. C. Soriano, and R. Zambrini, “Time-series quantum reservoir computing with weak and projective measurements,” *Npj Quantum Inf.*, vol. 9, no. 1, Feb. 2023.
- [16] J. Chen, H. I. Nurdin, and N. Yamamoto, “Temporal information processing on noisy quantum computers,” *Phys. Rev. Appl.*, vol. 14, p. 024065, Aug 2020. [Online]. Available: <https://link.aps.org/doi/10.1103/PhysRevApplied.14.024065>
- [17] K. Fujii and K. Nakajima, “Harnessing disordered-ensemble quantum dynamics for machine learning,” *Phys. Rev. Appl.*, vol. 8, no. 2, Aug. 2017.
- [18] K. Nakajima, K. Fujii, M. Negoro, K. Mitarai, and M. Kitagawa, “Boosting computational power through spatial multiplexing in quantum reservoir computing,” *Phys. Rev. Appl.*, vol. 11, no. 3, Mar. 2019.
- [19] W. Maass, T. Natschläger, and H. Markram, “Real-time computing without stable states: a new framework for neural computation based on perturbations,” *Neural Comput.*, vol. 14, no. 11, pp. 2531–2560, Nov. 2002.
- [20] T. Yasuda, Y. Suzuki, T. Kubota, K. Nakajima, Q. Gao, W. Zhang, S. Shimono, H. I. Nurdin, and N. Yamamoto, “Quantum reservoir computing with repeated measurements on superconducting devices,” 10 2023.
- [21] E. Bäumer, V. Tripathi, D. S. Wang, P. Rall, E. H. Chen, S. Majumder, A. Seif, and Z. K. Minev, “Efficient long-range entanglement using dynamic circuits,” *PRX Quantum*, vol. 5, p. 030339, Aug 2024. [Online]. Available: <https://link.aps.org/doi/10.1103/PRXQuantum.5.030339>
- [22] M. C. Mackey and L. Glass, “Oscillation and chaos in physiological control systems,” *Science*, vol. 197, no. 4300, pp. 287–289, Jul. 1977.
- [23] Y. Suzuki, Q. Gao, K. C. Pradel, K. Yasuoka, and N. Yamamoto, “Natural quantum reservoir computing for temporal information processing,” *Sci. Rep.*, vol. 12, no. 1, p. 1353, Jan. 2022.
- [24] Z. Liao, H. Yamahara, K. Terao, K. Ma, M. Seki, and H. Tabata, “Short-term memory capacity analysis of $\text{Lu}_3\text{Fe}_4\text{Co}_0.5\text{Si}_0.5\text{O}_{12}$ -based spin cluster glass towards reservoir computing,” *Scientific Reports*, vol. 13, no. 1, p. 5260, 2023. [Online]. Available: <https://doi.org/10.1038/s41598-023-32084-8>
- [25] Y. Li, K. Hu, K. Nakajima, and Y. Pan, “Composite force learning of chaotic echo state networks for time-series prediction,” in *2022 41st Chinese Control Conference (CCC)*. IEEE, Jul. 2022, p. 7355–7360. [Online]. Available: <http://dx.doi.org/10.23919/CCC55666.2022.9901897>
- [26] L. Appeltant, M. C. Soriano, G. Van der Sande, J. Danckaert, S. Massar, J. Dambre, B. Schrauwen, C. R. Mirasso, and I. Fischer, “Information processing using a single dynamical node as complex system,” *Nat. Commun.*, vol. 2, no. 1, p. 468, Sep. 2011.
- [27] M. C. Bañuls, J. I. Cirac, and M. B. Hastings, “Strong and weak thermalization of infinite nonintegrable quantum systems,” *Phys. Rev. Lett.*, vol. 106, p. 050405, Feb 2011. [Online]. Available: <https://link.aps.org/doi/10.1103/PhysRevLett.106.050405>
- [28] H. Jaeger, “The “echo state” approach to analysing and training recurrent neural networks-with an erratum note,” *Bonn, Germany: German national research center for information technology gmd technical report*, vol. 148, no. 34, p. 13, 2001.
- [29] K. Fujii and K. Nakajima, “Harnessing disordered-ensemble quantum dynamics for machine learning,” *Phys. Rev. Appl.*, vol. 8, p. 024030, Aug 2017. [Online]. Available: <https://link.aps.org/doi/10.1103/PhysRevApplied.8.024030>
- [30] J. Chen and H. I. Nurdin, “Learning nonlinear input–output maps with dissipative quantum systems,” *Quantum Inf. Process.*, vol. 18, no. 7, Jul. 2019.
- [31] M. Lukoševičius, *A Practical Guide to Applying Echo State Networks*. Springer Berlin Heidelberg, 2012, p. 659–686. [Online]. Available: http://dx.doi.org/10.1007/978-3-642-35289-8_36